ACS OMEGA

Open Access

http://pubs.acs.org/journal/acsodf

Article

Conductivity-Based Gas Sensors Using *Tamarindus indica* Polysaccharide-Capped Gold Nanoparticles for the Detection of Volatile Gases

Sumitha Selvanayakam, Saravana Priya Esakkidurai, and Swarnalatha Kalaiyar*

Cite This: *ACS Omega* 2024, 9, 10640−10649

Read Online

ACCESS | Metrics & More | Article Recommendations | Supporting Information

ABSTRACT: Gold nanoparticles (*n*Au) were synthesized by a sustainable approach utilizing tamarind seed polysaccharide (TSP). Polysaccharides are naturally occurring polymers derived from tamarind seeds, which function both as capping and reducing agents. Polyaniline (PANI) was subsequently capped over the as-prepared gold nanoparticles in order to facilitate the sensor property. The TSP-*n*Au-PANI film was fabricated by Methods I and II and utilized in the investigation of active sensor devices for the detection of organic pollutants such as benzene, toluene, and chloroform. The synthesized gold nanoparticles and the TSP-*n*Au-PANI films were analyzed using several analytical and spectral tools. Among the two methods, the Method II (TSP-*n*Au-PANI) film has a high sensing response toward benzene (105.69%), toluene (96.99%), and chloroform (74.98%). TSP is also a proton-conducting biopolymer, which enhances the conductivity of the material. The combination with the PANI layer of the film adsorbs the vapors easily and the prepared film material is more effective and ideal for sensing toxic gases.

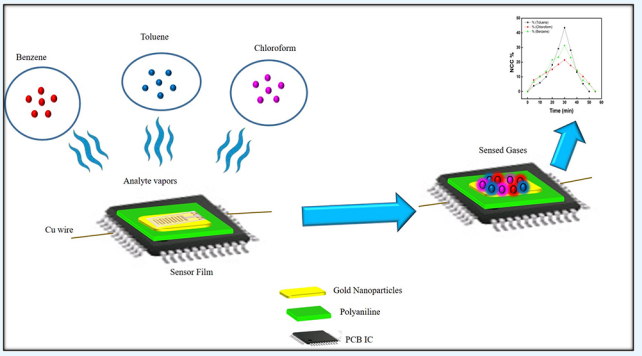

1. INTRODUCTION

Significant environmental pollutants with high neurotoxicity are volatile organic compounds (VOCs), which are often used as chemical reagents in industrial operations.[1,2] The majority of VOCs are dangerous and have been related to emphysema, cancer, allergies, and asthma.[3−5] The effectiveness of the gas sensor operating at typical temperature conditions was enhanced to effectively identify and measure potentially harmful gases present in low concentrations while accounting for diverse environmental conditions. Improvements in gas sensing technology necessitate the incorporation of cost-effectiveness, ecological compatibility, chemical stability, and long-term viability. Researchers are currently engaged in the active pursuit of developing signature sensors.[6,7] Gas sensors function by detecting alterations in electrical conductivity that occur due to the introduction of gas.[8]

In recent times, there has been a notable superiority of conductive-polymer-based sensors over metal-oxide-based sensors in terms of sensitivity, simplicity, and performance at room temperature. PANI is the preferred conductive polymer because of its distinctive qualities, including adaptable electrical and chemical properties, ease of manufacture, and low cost.[9−11] The utilization of polymers as a host for the encapsulation of metal nanoparticles has demonstrated its suitability, making composites composed of these materials highly advantageous. This is due to the amalgamation of the electrical properties inherent in metals with the mechanical attributes and ease of manipulation associated with polymers.[12,13] In contemporary companies focused on device technology, the synthesis of nanocomposites at a cheap cost is of utmost importance, as both the materials utilized and the manufacturing process play a crucial role. Various areas, including optoelectronics, memory, microelectronics, and sensors, employ such devices.[14,15] Currently, many researchers are working on nanocomposite gas detection sensors.[16] The environment provides natural polymers, including silk, wool, DNA, cellulose, carbohydrates, and proteins.[17−19] Polysaccharides are biological polymers made of monomeric sugars.[20] The tamarind tree (Tam Meus Indica L) is commonly planted in the arid parts of central and southern India along with other countries in the western region of South Asia since its commercial value enhances its importance. Tamarind seed polysaccharide (TSP) has good viscosity, a broad pH tolerance range, noncarcinogenicity, mucosal adherence, and biocompatibility.[21] TSP has a backbone of (1 → 4)-*β*-D-glucan modified

Received: November 16, 2023
Revised: January 26, 2024
Accepted: February 1, 2024
Published: February 24, 2024

with a side chain of α-D-xylopyranose and a linkage of α-D-galactopyranose (1 → 2)-β-D-glucose (1 → 6).[22,23] Scientists and engineers focus on nanomaterials because of their unique properties, such as optical, magnetic, and electrical properties. These unique traits may benefit electronics, spintronics, medical applications, and other technical products too.[24,25]

Polymer, dendrimer, liposome, and metal nanoparticles have been extensively studied for drug delivery, biodegradation, and biosensors.[26,27] Gold nanoparticles have garnered attention and intensive research. Gold nanoparticles transport and unload medicines using their chemical and physical characteristics. The gold core is inert and nontoxic.[28,29] Single-disperse nanoparticles with core diameters from 1 to 150 nm are easy to synthesize. Researchers can choose from colloidal gold nanoparticles, nanorods, silica/gold nanoshells, nanotubes, nanorices, nanostars, or nanocages. Several investigations have used plant extracts for the synthesis of nanomaterials, for e.g., *Lawsonia intermis*, *Sphaeranthus indicus*, *Carica papaya*, *Ocimum sanctum*, *Piper longum*, *Rhus chinensis*, *Polyscias scutellaria*, *Stachys lavandulifolia Vahl*, etc.[30−33] However, AuNPs were synthesized by chemical reduction with $NaBH_4$, and TSP blended with chitosan was used as the capping agent.[34] Though there are many green methods for the synthesis of Au NPs, synthesis of polysaccharide-capped gold nanoparticles particularly with TSP is limited.

The current study aimed to synthesize nanogold utilizing a green method using polysaccharides as the capping and reducing agents. The synthesized AuNPs were tested for chemosensor sensitivity using PANI as the conductive polymer.

2. EXPERIMENTAL SECTION

2.1. Materials and Methods. Tamarind seeds were obtained from Kunnathoor village in Kanyakumari district of Tamil Nadu. The chemical reagents chloroauric acid ($HAuCl_4$), propanol (GR), and methanol (AR) were purchased from Loba Chemie, India. Hydrochloric acid (HCl), sodium hydroxide (NaOH), aniline (99.5%), ammonium peroxodisulfate (98%), toluene (GR) (99.5%), and benzene (GR) were procured from Merck Specialties Private Limited, Mumbai. Chloroform (99%) (AR) was obtained from Rankem RFCL Private Ltd. located in New Delhi, India.

2.1.1. Isolation of Tamarind Seed Polysaccharide. The standard protocol already reported for the isolation of TSP has been modified and followed.[35] The obtained seeds of *Tamarindus indica* were cleansed with deionized water to remove the adhering materials and dried under shadow. The maroon-colored outer cover (testa) of the tamarind seeds was removed by applying mechanical force. The off-white portion (kernel) of the seeds was crushed to small granules and then pulverized to a fine powder with a household mixer grinder. This tamarind kernel powder was purified by washing repeatedly and successively with 0.1 M HCl, 0.1 M NaOH, methanol, and propanol and finally with DDW to remove unwanted chemical components like protein, etc. Purified TSP powder was then dried in an air oven at 60 °C. The obtained thick mass was crushed to coarse powder with a mortar and pestle and stored in a zip-lock polythene cover for further studies.

2.1.2. Synthesis of Nanogold. 200 mg of TSP powder was added to 50 mL of DDW, stirred, and heated. After complete dissolution, 9 mg of chloroauric acid was added to this viscous solution, and the whole mixture was stirred for about 5 min to achieve the reduction of gold tripositive ions. The yellow color of the mixture changed to wine red, indicating the formation of AuNPs.

2.1.3. Synthesis of PANI. The synthesis was carried out by utilizing in situ chemical oxidative polymerization. 20 μL of 0.1 M aniline in 0.2 M HCl supplied through a micropipette (10−100 μL Finnpipett) was placed on a watch glass. Then, 20 μL of ammonium peroxodisulfate in 0.2 M HCl was added and mixed well. The solution was left alone for roughly 1 h for polymerization. A thin coating of polyaniline (PANI) was created on the printed circuit board (PCB) as a result of polymerization.

2.2. Characterization. The ultraviolet−visible (UV−vis) spectrum of AuNPs was recorded using a PerkinElmer Lambda 25 spectrophotometer in the 200−800 nm range. The Fourier transform infrared (FT-IR) spectrum was recorded with a JASCO FT-IR 410 spectrophotometer in the 500−4000 cm^{-1} range (KBr pellet technique). The X-ray diffraction (XRD) patterns were obtained with a PANalytical Expert Pro-MPG X-ray diffractometer using a Cu Kα radiation source (λ = 1.5406 Å) at 2θ = 10−80°. The morphology of *n*Au was examined by scanning electron microscopy (SEM, ZEISS EVO 18) images. Energy-dispersive X-ray (EDX) spectroscopy analysis was performed on a Bruker instrument.

2.3. Sensor Functionality. PANI and PANI-TSP/AuNP material films were the subject of a study on the materials' sensor capability. Each of these material films was individually subjected to the solvent vapors of benzene, toluene, or chloroform for 30 min. The solvent was evaporated under normal air pressure in the absence of vacuum, and the experimental condition was comparable to the field condition.

2.3.1. Preparation of the Sensor via a Thin Film. The sensor device was made using a printed circuit board (PCB), which was inexpensive and simple to make. The PCB was divided into sections that were roughly 1 cm square. From the bottom of the PCB, two adjacent holes were used to insert two prepolished copper wires that served as two probes for the sensor tests. These wires were soldered to the PCB at two adjacent metal contact points at a distance of 0.3 cm (3 mm) between them. The PCB with these two soldered contact points was utilized for the subsequently described deposition of the conducting polymer material. *In situ* chemical oxidative polymerization was carried out in the synthesis. The sensor device was fabricated by already reported literature.[36] Three types of sensor film materials were prepared by Method I, Method II, and PANI.

2.3.1.1. Method I. In Method I, 50 μL of a fresh mixture containing 40 μL of PANI and 10 μL of *n*Au was added to the watch glass and mixed well, and polymerization occurred. Then, using a micropipet, 50 μL of the mixed solution was instantly coated over the PCB and allowed to stand for an uninterrupted hour. The two soldering points on the PCB were then covered with conductive Ag paste (rather than the sensor material that had been placed), ensuring a good ohmic contact between the polymeric film and the copper-soldered points.

2.3.1.2. Method II. In Method II, the same composition of PANI and *n*Au was taken. 40 μL of PANI was the first-layer film over the PCB dried and 10 μL of *n*Au was the second layer over PANI and was allowed to stand without disturbance for about 1 h for drying. Then, the same procedure adopted in Method I was followed.

2.3.1.3. PANI Film. 40 μL of PANI (20 μL of 0.1 M aniline + 20 μL of APS) was coated over the PCB and allowed to

https://doi.org/10.1021/acsomega.3c09137
ACS Omega 2024, 9, 10640−10649

stand without any disturbance for about 1 h for polymerization. In order to prepare the PANI film, copper-soldered points and conductive Ag paste were simply applied over the soldering areas on the PCB.

2.3.2. Conductivity and Sensor Experiments. A glass vacuum desiccator was utilized to construct a sensor chamber with a volume of 900 mL, featuring specific apertures for the introduction and release of gases. The experimental setup consisted of a vessel containing a solvent, two copper wires with silver bonded probes, and a printed circuit board (PCB) coated with a film of sensor material (polyaniline) using either Method I or Method II. These components were assembled and placed in a chamber for further experimentation. The MIC 16 H digital multimeter was used to test the resistance of the PCB-covered sensor material at room temperature.

The assessment of the sensor's effectiveness in the printed circuit board (PCB) device was performed by evaluating the alteration in resistance when exposed to analyte vapor. This measurement was performed at 5 min intervals, for a total duration of 30 min within each cycle. Three experimental response−recovery cycles were performed to analyze the vapor of the analyte or air. In each cycle, the change in resistance was observed at 5 min intervals. The calculation of the sensor function/response for each cycle involved the use of eq 1 to determine the normalized conductivity change % (NCC%).

$$\text{NCC\%} = \frac{R_{\text{Ana}} - R_{\text{Air}}}{R_{\text{Air}}} \times 100 \quad (1)$$

where R_{Ana} = resistance in the analyte and R_{Air} = resistance in air. NCC percentages were determined for each 5 min interval. All three cycles averaged these values. The sensor function analysis used only the average NCC% values.

3. RESULTS AND DISCUSSION

3.1. FT-IR Characterization of the Samples. The TSP biopolymer shows (Figure 1a) a high intense broad band around 3600 cm^{-1}, two stepwise less intense bands around 3300 and 3200 cm^{-1} (all three due to O−H stretching), one high intense and two weak bands at 3000, 2800, and 2700 cm^{-1} (all due to −C−H stretching in the glucan backbone and aldehyde, O=C−H groups), a similar high intense band at 1750 cm^{-1} due to the carbonyl group, three consecutive moderate intense peaks assignable to −C−H bending in the 1500−1350 cm^{-1} range, another three moderate intense peaks in the 1200−1000 cm^{-1} range due to C−O stretching, and finally a single weak peak at almost 750 cm^{-1} appearing by −C−H rock vibration. This FT-IR spectrum confirms the purity of TSP, which is well correlated with the previous reports.[37]

The vibrational bands/peaks of TSP undergo substantive changes in forming *n*Au. First, the three −O−H stretch bands merge into a single V-shaped band and appear at a red-shifted position (3400 cm^{-1}) (Figure 1b). Second, the C−H band almost completely disappears. Third, the carbonyl, C−H bending, and C−O stretch bands all appear at the lower wavenumber side with a reduction in intensity. All of these changes reported already[31,39] prove that there is a strong interaction between TSP and Au^{3+}/*n*Au and that the respective chemical groups of TSP perform the reduction of Au^{3+} ion and the capping and stabilizing functionalities. The FT-IR spectrum of TSP/*n*Au/PANI is shown in Figure 1c. It shows that a major characteristic peak at 3450 and 1986 cm^{-1} is similar to that of standard PANI reported in the literature.[36,38]

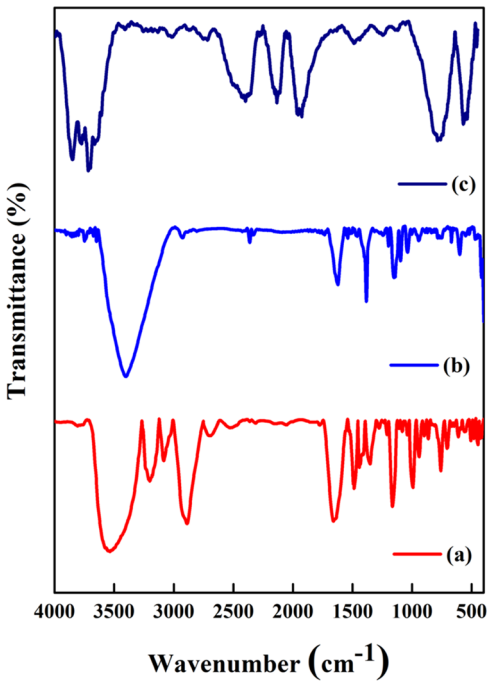

Figure 1. FT-IR spectra of (a) TSP, (b) TSP/*n*Au, and (c) TSP/*n*Au/PANI.

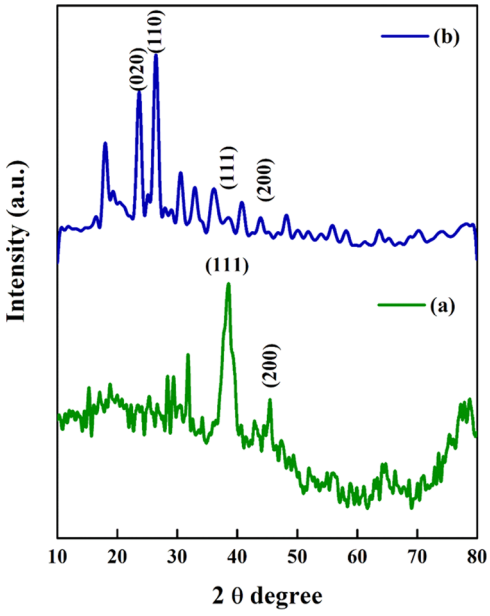

Figure 2. XRD patterns of (a) TSP/*n*Au and (b) TSP/*n*Au/PANI.

The peak corresponding to 525 cm^{-1} reveals the stretching of the group of films (*n*Au).

3.2. XRD. The film-coated and oven-dried TSP/*n*Au sample was used for XRD characterization (Figure 2a). Two diffraction peaks appear at 2θ = 38.34 and 45.28°, which coincide with the earlier reports[31,38] and also with JCPDS file no. 04-0784, yielding the inference that the present *n*Au have face-centered cubic (fcc) crystal structures. The peaks are assigned to (111) and (200) planes of the fcc lattice. The average crystallite size obtained by the Debye−Scherrer method is 4.29 nm. Besides these two explicit peaks, the XRD pattern also shows broad signals around 20 and 30°, characteristic for TSP, implying that TSP has an amorphous

https://doi.org/10.1021/acsomega.3c09137
ACS Omega 2024, 9, 10640−10649

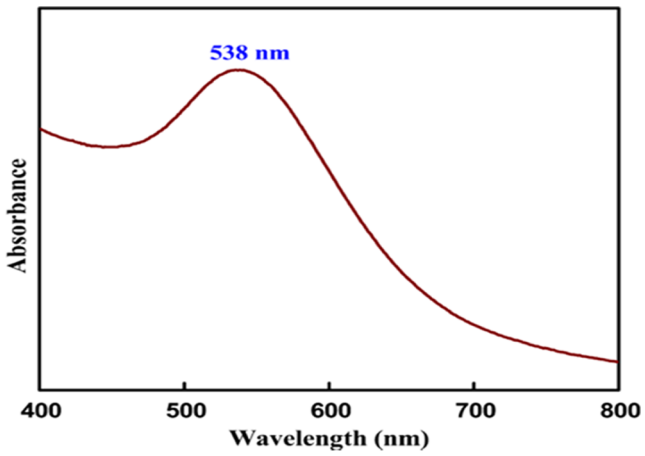

Figure 3. UV-visible spectrum of TSP/*n*Au.

structure.[39] Figure 2a displays the powder XRD patterns of TSP and *n*Au. Figure 2b shows that TSP/*n*Au/PANI and PANI exhibit the signals at about 23.63 and 26.40°, which are matchable with literature data[38] and also with JCPDS file no. 09-0432. The peaks are assigned to (020) and (110) planes of the fcc lattice.

3.3. UV. A color change was apparent within minutes, confirming the cross-linking of the AuNPs due to the expected change in plasmon resonance. The solution was allowed to react (cross-link) for few more minutes (~10 min), a colloidal solution of nanoparticles was formed. The color change of the UV−visible absorption spectrum confirms the formation of the nanoparticles in aqueous solution. Absorption spectra of the NPs (538 nm) were acquired throughout the cross-linking process to observe the changes in plasmon resonance.[40] A shift correlates to a change in resonance attributed to the cross-linking of the NPs. These shifts are observed in the spectra displayed in Figure 3.

3.4. Scanning Electron Microscopy. The SEM images of TSP/*n*Au (Figure 4a) show the agglomerated spherical-shaped particles. The size of the spheres was measured in nanometers. The nanospheres have variant sizes of 27.3, 36, 44, 50, and 55.7 nm due to TSP. TSP/*n*Au has agglomerated morphology, shown in Figure 4a, and a similar morphology is observed for the TSP-chitosan *n*Au composite.[34] In the case of Method II, TSP/*n*Au/PANI shows the flowerlike structures in micrometers, and there is no agglomeration because there are PANI features included, which are clearly visible. SEM reveals a transition from agglomerated to smooth flowerlike morphology, as seen in the root of PANI thin films. There is an interaction of PANI and gold nanoparticle surface plasmon resonance. But some morphology was changed due to the conductivity material of PANI. Figure 4b also shows the polymerization of aniline over TSP/*n*Au particles and the resultant coating/coverage over TSP/*n*Au.

Table 1. EDX Data of TSP/*n*Au

element	atomic number	mass (%)	mass normalized (%)	atom (%)
carbon	6	25.36	41.38	57.42
oxygen	8	19.02	31.03	32.33
gold	79	7.09	11.57	0.98

3.5. Energy-Dispersive X-ray (EDAX) Analysis. The elemental composition of TSP-*n*Au was analyzed using SEM-EDX, and the resulting data have been recorded in Table 1 and is depicted in Figure 5a. In addition to the typical elements of carbon, hydrogen, and oxygen, the presence of chlorine and gold was also observed. Gold is found in trace amounts, specifically at a concentration of 0.98 atom %. The electron diffraction (EDX) pattern, depicted in Figure 5b, provides evidence of the existence of carbon, nitrogen, and oxygen. This observation supports the production of polyaniline (PANI) and aligns with the information recorded in Table 2.

3.6. Determination of VOC Vapors. In a gas detection chamber, saturated vapor was created at ambient temperature in a 5 mL beaker with 1 mL of sample liquid. For each experiment, one gas was chosen from benzene, toluene, and chloroform. The PANI and Method I/II sensor material films

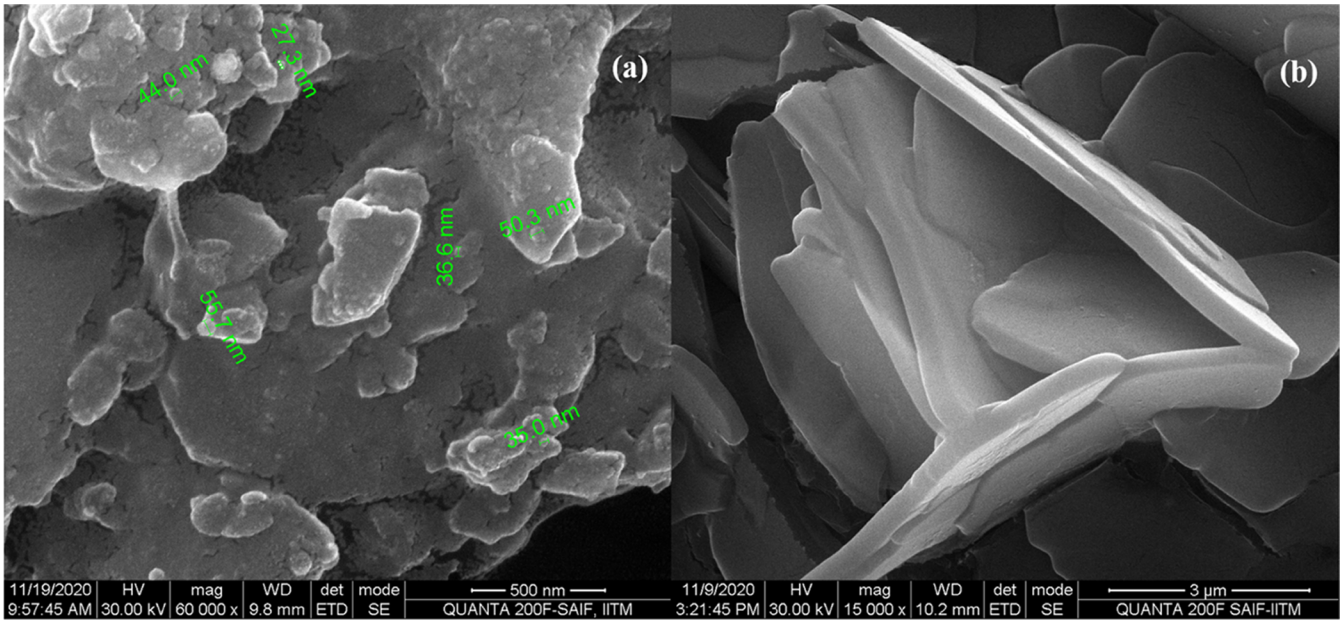

Figure 4. SEM images of (a) TSP/*n*Au and (b) TSP/*n*Au/PANI.

https://doi.org/10.1021/acsomega.3c09137
ACS Omega 2024, 9, 10640−10649

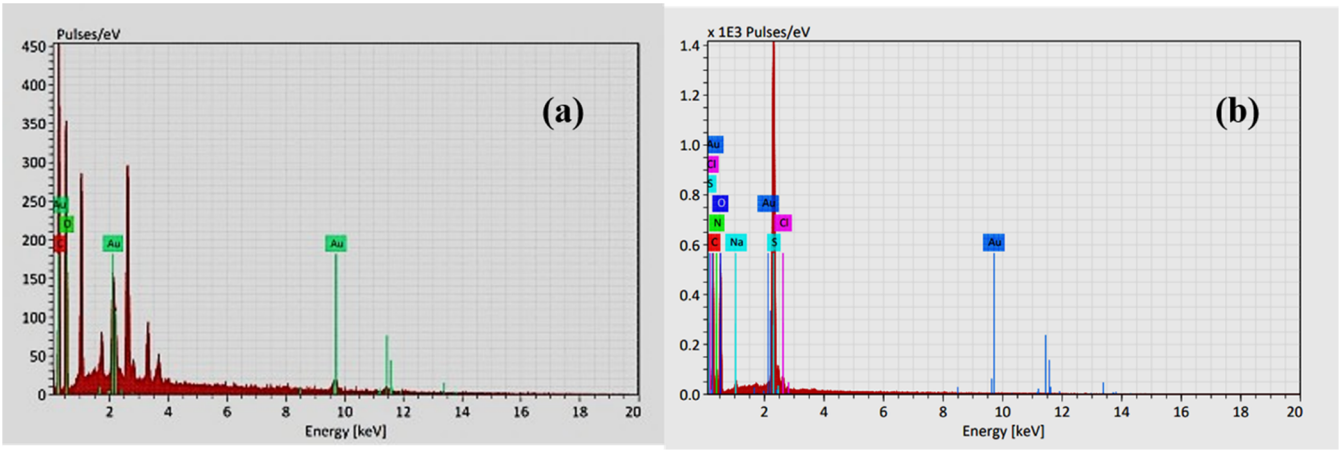

Figure 5. Elemental analysis of (a) TSP/*n*Au and (b) TSP/*n*Au/PANI.

Table 2. EDX Data of TSP/AuNPs/PANI

element	atomic number	mass (%)	mass normalized (%)	atom (%)
carbon	6	40.06	35.53	**44.94**
nitrogen	7	15.84	14.05	**15.24**
oxygen	8	37.93	33.64	**31.94**
sodium	11	0.67	0.59	**0.39**
sulfur	16	17.03	15.10	**7.16**
chlorine	17	0.78	0.69	**0.30**
gold	79	0.46	0.41	**0.03**

Table 3. Sensor Functionality (NCC%) of the Materials

	NCC%		
sample	benzene	toluene	chloroform
PANI	31.32	43.39	21.49
Method I	39.81	44.52	25.79
Method II	105.69	96.99	74.98

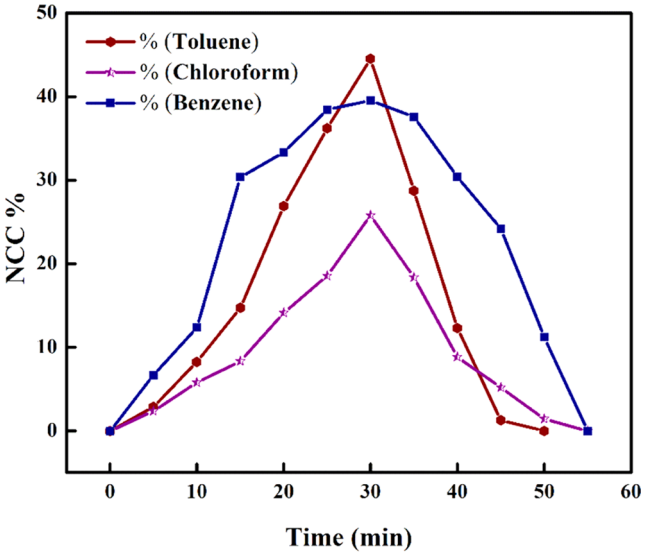

Figure 6. Sensor responses of BTC gas sensing by Method I.

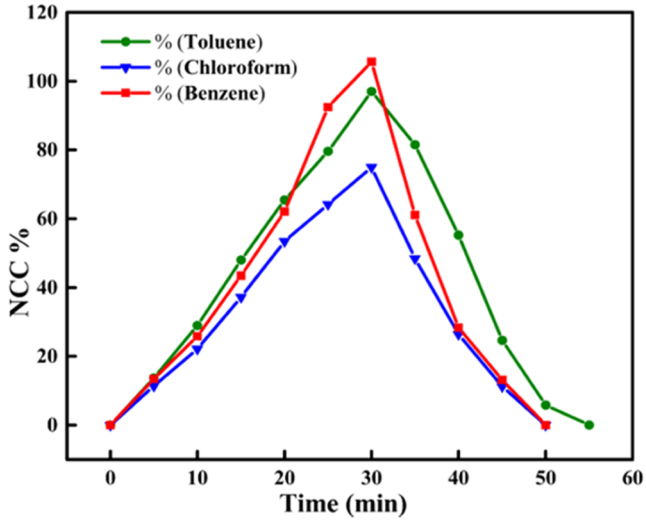

Figure 7. Sensor responses of BTC gas sensing by Method II.

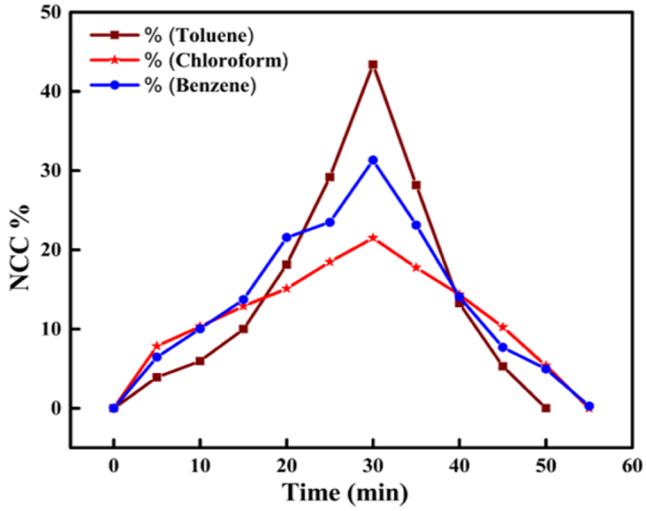

Figure 8. Sensor responses of BTC gas sensing by PANI.

were coupled to a multimeter (MIC 16 H digital multimeter) to record resistance/impedance responses while alternating the exposure of the sample VOC vapor with fresh air. Detection cycles can be repeated three times. After the chamber's air is replaced, the above procedure is repeated to measure another sample. The PANI film shows the sensing response of benzene, toluene, and chloroform vapor containing 31, 43, and 21%. Pure nanogold's low conductivity limits its sensor effectiveness. PANI also shows very meager sensitivity toward benzene, chloroform, and toluene fumes. Two methods were used to

https://doi.org/10.1021/acsomega.3c09137
ACS Omega 2024, 9, 10640−10649

Table 4. Weight Loss of Benzene, Toluene, and Chloroform during Solvent Evaporation

	weight loss in benzene				weight loss in toluene				weight loss in chloroform			
time (min)	exp no. 1 (mg)	exp no. 2 (mg)	avg (mg)	con (ppm)	exp no. 1 (mg)	exp no. 2 (mg)	avg (mg)	con (ppm)	exp no. 1 (mg)	exp no. 2 (mg)	avg (mg)	con (ppm)
5	29.3	29.4	29.35	32.61	12.3	11	11.65	12.94	95.6	90.2	92.9	103.22
10	49.2	48.4	48.8	54.22	17.7	18	17.85	19.83	142.3	157.9	150.1	166.78
15	63.0	65.3	64.15	71.28	23.0	23.6	23.3	25.89	192.6	201.9	197.25	219.17
20	79.3	78.3	78.8	87.55	30.9	31.8	31.35	34.83	243.7	253.9	248.8	276.44
25	97.3	93	95.15	105.72	36.6	35.1	35.85	39.83	277.6	290.6	284.1	315.67
30	107.2	113.9	110.55	122.83	39.4	39.1	39.25	43.61	317.7	329.4	323.55	359.5

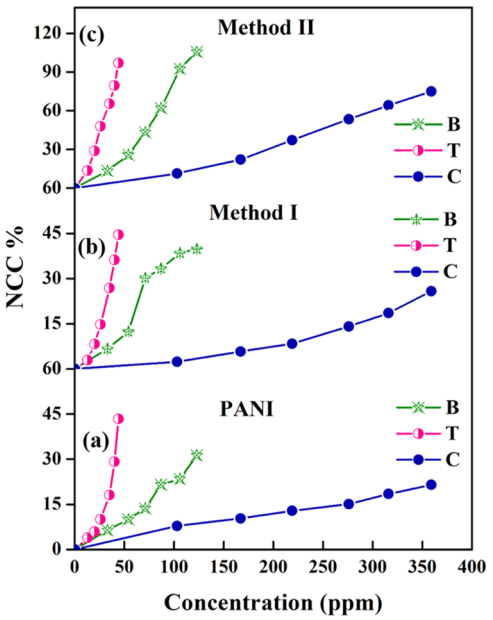

Figure 9. Sensor functionality of the materials: (a) PANI, (b) Method I, and (c) Method II in BTC atmospheres.

Table 5. Weight Loss of Benzene and Toluene during Solvent Evaporation

	weight loss in benzene + toluene in separate container				weight loss in benzene + toluene in single container	
			con (ppm)			con (ppm)
time (min)	*B* (mg)	*T* (mg)	*B*	*T*	*B* + *T* (mg)	*B* + *T*
5	19	3	**21**	**3**	14	**16**
10	34	9	**38**	**10**	24	**26**
15	52	15	**58**	**17**	37	**41**
20	73	21	**81**	**23**	48	**53**
25	89	27	**99**	**30**	61	**68**
30	111	34	**123**	**38**	77	**86**

study the PANI and *n*Au composite sensor activity. Method I mixed the form of TSP/*n*Au with PANI composites. The sensor response of benzene, toluene, and chloroform is 39, 44, and 25%, respectively. This methodology shows average sensing responses and the interaction of analytes having huge conductivity. The second methodology of Method II coats and dries the PANI layer first, followed by coating the nanogold layer second. Method II shows an NCC% of 105.69, showing the sensor's sensitivity to benzene analyte vapors at 118 ppm via reducing conductivity to the interaction of analyte vapors. Toluene and chloroform contain 96% and 74% nitrogen-containing compounds, respectively.

Table 6. Weight Loss of Benzene and Chloroform during Solvent Evaporation

	weight loss in benzene + chloroform in separate container				weight loss in benzene + chloroform in single container	
			con (ppm)			con (ppm)
time (min)	*B* (mg)	*C* (mg)	*B*	*C*	*B* + *C* (mg)	*B* + *C*
5	20	45	**22**	**50**	43	**48**
10	33	93	**36**	**103**	85	**94**
15	56	139	**62**	**154**	130	**144**
20	73	189	**81**	**210**	166	**184**
25	92	233	**102**	**259**	220	**244**
30	112	290	**124**	**322**	262	**291**

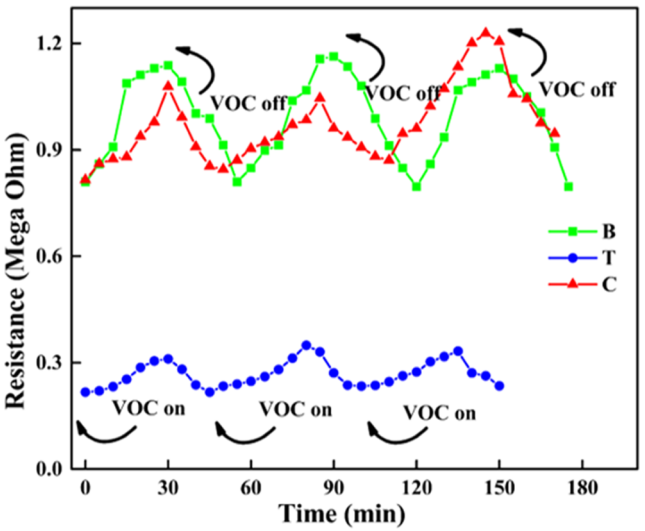

Figure 10. Dynamic profile of gas sensing by Method I.

Method II involved the chemical detection of analytes by the PANI layer, and also TSP is a proton-conducting polymer. The interaction of two polymers and the surface plasmon resonance in the nanogold's second layer absorb vapor signals and increase conductivity through electron transitions. The printed circuit board was responsible for the acquisition of electrical impulses. The sensors also respond differently to analyte concentration. Table 3 shows the sample TSP-*n*Au-PANI data. Static sensor activity is rapid, reversible, and regenerative across all materials. When analyte vapor is replaced with ambient air, material conductivities return to their initial values. A representative TSP-*n*Au-PANI composite sample was investigated for dynamic sensor qualities to confirm and explain this observation. Figure 6 of Method I, Figure 7 of Method II, and Figure 8 of PANI show response−recovery curves for benzene, toluene, and chloroform. After 5 min of

https://doi.org/10.1021/acsomega.3c09137
ACS Omega 2024, 9, 10640−10649

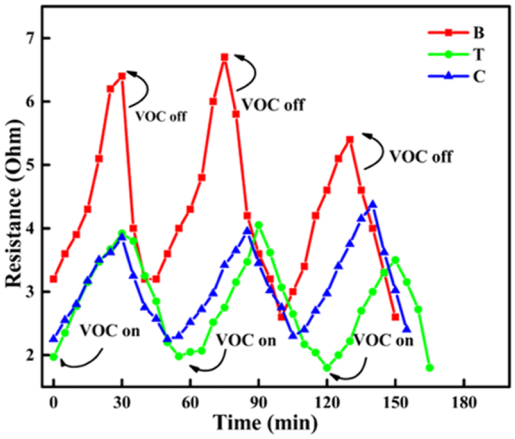

Figure 11. Dynamic profile of gas sensing by Method II.

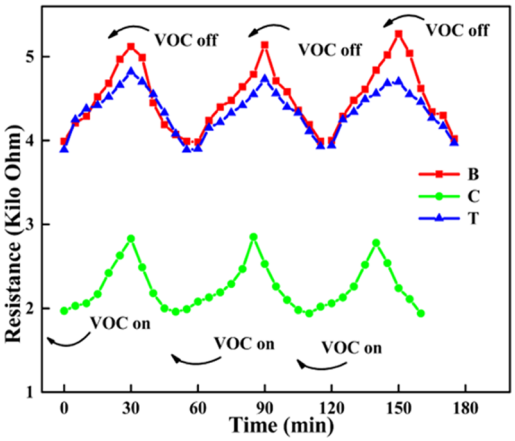

Figure 12. Dynamic profile of gas sensing using PANI.

exposure to BTC gases, the material approaches saturation and achieves maximum sensing capabilities (as shown by a rise in voltage or a decrease in conductivity). When the BTC gases evaporate, the material returns to its initial value in 10 min. Cycles 2 and 3 show the same profile as cycle 1, suggesting sensor material reversibility, recovery, and regeneration. For each vapor, the mean NCC% values were determined.

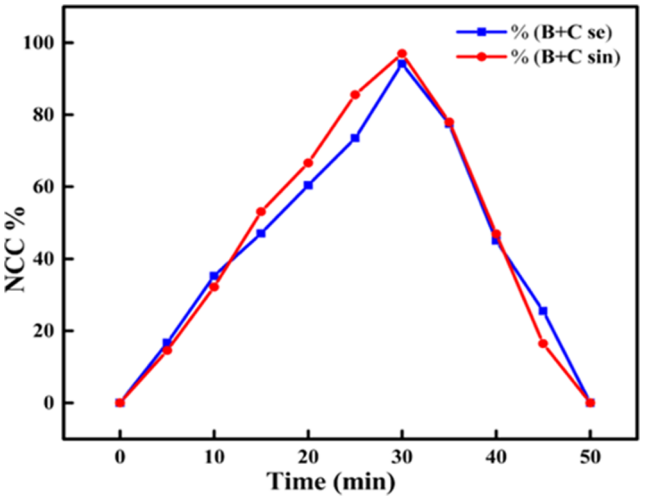

Figure 14. Sensor responses of the mixture of vapors ($B + C$) in single and separate containers of Method II.

Toluene and chloroform concentrations are lower than those of benzene under comparable conditions. Toluene has a boiling point (110.60 °C) higher than that of benzene (80.10 °C), which slows toluene evaporation. Chloroform's boiling point is 61.2 °C, having average sensor responses, by comparing the other two vapors. The solvent evaporation and vapor concentration rise linearly with time.

The sensitivity data of TSP-*n*Au-PANI at various concentrations of benzene, toluene, and chloroform are tabulated in Table 4 and Figure 9a−c demonstrate the sensor functioning of nanocomposite sensors, which depends on the analyte concentration and rapid reaction and recovery. Due to their complementarity and synergy, the *in situ* synthesis of PANI−*n*Au composites improves the sensor performance. Understanding this connection is essential to understanding the synergistic function and sensor efficiencies in composite materials.

Before the beginning of the sensor experiment, the analyte vapor concentration was studied separately for 30 min evaporation. The concentration data of the weight loss of benzene, toluene, and chloroform vapors during solvent evaporation are tabulated in Table 4. The concentration data of the mixture of solvents in single and separate containers (B

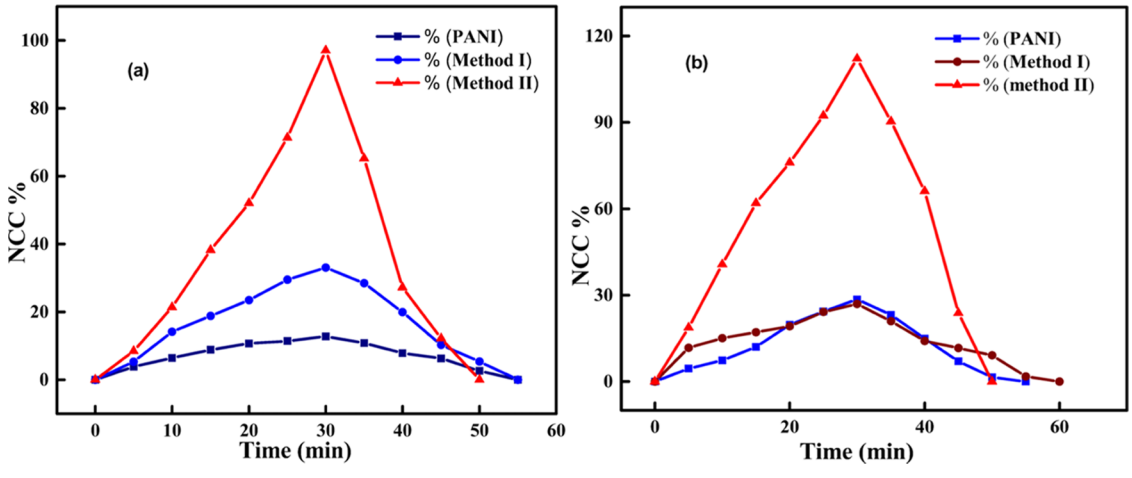

Figure 13. Sensor responses of the mixture of vapors ($B + T$) in (a) single and (b) separate containers of PANI, Method I, and Method II.

https://doi.org/10.1021/acsomega.3c09137
ACS Omega 2024, 9, 10640−10649

Table 7. Comparison of Sensor Materials for the Detection of VOCs

material	operating temperature (°C)	range of detection	VOC gases	response time	ref
SnO_2 (Cd)	225	0−500 ppm	ethanol	15−25 s	41
SnO_2 (gold NPs)	RT	10−120 ppm	ethanol	∼5 s	42
AgNPs	RT	0.54 μM, 0.032 μM, 0.29 μM	Fe^{2+}, H_2O_2, glucose	15 min	43
Au-SnO_2 HNS	250 °C	100 ppm	ethanol	200−500 s	44
C11TEA	20 ∘C	≥95%	chloroform, benzene, toluene, ethanol	20 min	45
PANI-SnO_2	RT	10%	benzene/toluene	15 min	3
TSP-AuNPs-PANI	RT	106%	benzene, toluene, chloroform	30 min	present work

+ T and B + C) are presented in Tables 5 and 6, and the concentration profiles are shown in Figure 9a−c. The vapor concentration calculation was tabulated using eq 2:

$$\text{weight loss of vapor (mg)}/900\ \text{mL} \times 1000\ \text{mL} = \text{concentration in ppm} \quad (2)$$

3.7. Dynamic Profile of PANI, Method I, and Method II. Polyaniline (PANI) has the lowest sensor functionality of the three films, while Method II has the highest. All film material sensors operate near-linearly with the analyte concentration. Chloroform has a lower sensor response than that of benzene and toluene. The three dynamic response−recovery patterns of sensor devices are depicted in Figures 10−12. The sensor observations and results suggest that the analyte and the sensor material interact physically, possibly via surface adsorption.

The sensor capabilities of mixed vapors containing benzene and toluene were evaluated using PANI, Method I, and Method II. The assessment was conducted both in a single container (Figure 13a) and separate containers (Figure 13b). The efficiency of Method II in all sensor responses is effective. Due to that reason, we assess the operational efficacy of sensors in detecting benzene and chloroform, both in single and separate (Figure 14) containers, utilizing Method II exclusively. The comparison of other sensor materials with the present work is presented in Table 7. The resusability and repeatability of the sensor film was analyzed and the data is given in Figure S1.

4. CONCLUSION

Gold nanoparticles were synthesized economically, and the utilization of tamarind seed polysaccharide has proven to be highly effective in its capacity as both reducing and stabilizing agents. Gold nanoparticles (*n*Au) were found as agglomerated clusters due to the presence of TSP. The sensitivity of AuNP-based sensors can be influenced by various parameters, such as the analyte, recognition partner, and transduction device. The PANI film material shows a very low sensor response compared to the other two films. The TSP-*n*Au-PANI film material of Method I shows an average sensing response. The effective sensor film material of Method II is a sandwich model sensor device fabricated to detect BTC gases. Among the three (BTC) gases, benzene having a high sensitivity of NCC% is 105.96 at ∼118 ppm concentration because the adsorption of benzene on the surface of the sensor is very high. The sensor efficiency of all of the materials and methods performed in normal conditions is an advantageous feature of the present materials.

■ ASSOCIATED CONTENT

Data Availability Statement

The data used to support the findings of this study are included within the article.

Supporting Information

The Supporting Information is available free of charge at https://pubs.acs.org/doi/10.1021/acsomega.3c09137.

Stability of the sensor film (PDF)

■ AUTHOR INFORMATION

Corresponding Author

Swarnalatha Kalaiyar − *Photochemistry Research Laboratory, Department of Chemistry, Manonmaniam Sundaranar University, Tirunelveli 627012 Tamil Nadu, India;* orcid.org/0000-0002-8009-6924; Email: swarnalatha@msuniv.ac.in

Authors

Sumitha Selvanayakam − *Photochemistry Research Laboratory, Department of Chemistry, Manonmaniam Sundaranar University, Tirunelveli 627012 Tamil Nadu, India*

Saravana Priya Esakkidurai − *Photochemistry Research Laboratory, Department of Chemistry, Manonmaniam Sundaranar University, Tirunelveli 627012 Tamil Nadu, India*

Complete contact information is available at: https://pubs.acs.org/10.1021/acsomega.3c09137

Notes

The authors declare no competing financial interest.

■ ACKNOWLEDGMENTS

The authors are thankful to the Department of Physics, Manonmaniam Sundaranar University, Tirunelveli-12, Tamil Nadu, India, for XRD measurements and the Indian Institute of Technology, Madras, Sophisticated Analytical Instrumental Facility, for SEM characterizations. This research did not receive any specific grant from funding agencies in the public, commercial, or not-for-profit sectors.

■ REFERENCES

(1) Huang, B.; Lei, C.; Wei, C.; Zeng, G. Chlorinated volatile organic compounds (Cl-VOCs) in Environment-sources, potential human health impacts, and current remediation technologies. *Environ. Int.* **2014**, *71*, 118−138.

(2) Sharma, S.; Meena, M.; Swapnil, P.; Marwal, A.; Gupta, A. K. Removal of Volatile Organic Compounds and Heavy Metals Through the Biological-Based Process. In *An Innovative Role of Biofiltration in Wastewater Treatment Plants (WWTPs)*; Elsevier, 2022; pp 45−64.

(3) Murugan, C.; Subramanian, E.; Padiyan, D. P. p−n Heterojunction formation in polyaniline−SnO_2 organic−inorganic

hybrid composite materials leading to enhancement in sensor functionality toward benzene and toluene vapors at room temperature. *Synth. Met.* **2014**, *192*, 106−112.
(4) Kotresh, S. T.; Ravikiran, Y.; Vijaya Kumari, S. C.; Raj Prakash, H. G.; Thomas, S. Polyaniline niobium pentoxide composite as humidity sensor at room temperature. *Adv. Mater. Lett.* **2015**, *6*, 641−645.
(5) Aranthady, C.; Shanbhag, G. V.; Sundaram, N. G. Polyaniline/(Ta_2O_5−SnO_2) hybrid nanocomposite for efficient room temperature CO gas sensing. *RSC Adv.* **2022**, *12*, 15759−15766.
(6) Ghule, B. G.; Shaikh, S.; Ekar, S. U.; Nakate, U. T.; Gunturu, K. C.; Shinde, N. M.; Mane, R. S.; et al. Natural carbonized sugar as a low-temperature ammonia sensor material: experimental, theoretical, and computational studies. *ACS Appl. Mater. Interfaces* **2017**, *9*, 43051−43060.
(7) Sugunan, A.; Dutta, J. Pollution treatment, remediation and sensing. *Nanotechnology* **2008**, *3*, 125−143.
(8) Raya, I.; Kzar, H. H.; Mahmoud, Z. H.; Al Ayub Ahmed, A.; Ibatova, A. Z.; Kianfar, E. A review of gas sensors based on carbon nanomaterial. *Carbon Lett.* **2021**, 1−26.
(9) Rahimi, R.; Ochoa, M.; Tamayol, A.; Khalili, S.; Khademhosseini, A.; Ziaie, B. Highly stretchable potentiometric pH sensor fabricated via laser carbonization and machining of Carbon−Polyaniline composite. *ACS Appl. Mater. Interfaces* **2017**, *9*, 9015−9023.
(10) Sumdani, M. G.; Islam, M. R.; Yahaya, A. N. A.; Safie, S. I. Recent advancements in synthesis, properties, and applications of conductive polymers for electrochemical energy storage devices: A review. *Polym. Eng. Sci.* **2022**, *62*, 269−303.
(11) Sadek, A. Z. M. Investigation of Nanostructured Semiconducting Metal Oxide and Conducting Polymer Thin Films for Gas Sensing Applications. Doctoral Dissertation, RMIT University, 2008.
(12) Hatchett, D. W.; Josowicz, M. Composites of intrinsically conducting polymers as sensing nanomaterials. *Chem. Rev.* **2008**, *108*, 746−769.
(13) Biswas, M. C.; Chowdhury, A.; Hossain, M. M.; Hossain, M. K. Applications, Drawbacks and Future Scope of Nanoparticles-Based Polymer Composites. In *Nanoparticle-Based Polymer Composites*; Woodhead Publishing, 2022; pp 243−275.
(14) Sanchez, C.; Belleville, P.; Popall, M.; Nicole, L. Applications of advanced hybrid organic−inorganic nanomaterials: from laboratory to market. *Chem. Soc. Rev.* **2011**, *40*, 696−753.
(15) Mazari, S. A.; Ali, E.; Abro, R.; Khan, F. S. A.; Ahmed, I.; Ahmed, M.; Shah, A.; et al. Nanomaterials: Applications, waste-handling, environmental toxicities, and future challenges—A review. *J. Environ. Chem. Eng.* **2021**, *9*, No. 105028.
(16) Pavase, T. R.; Lin, H.; Hussain, S.; Li, Z.; Ahmed, I.; Lv, L.; Kalhoro, M. T.; et al. Recent advances of conjugated polymer (CP) nanocomposite-based chemical sensors and their applications in food spoilage detection: A comprehensive review. *Sens. Actuators, B* **2018**, *273*, 1113−1138.
(17) Bhatia, S. Natural polymers vs synthetic polymer. *Nat. Polym. Drug Delivery Syst.* **2016**, 95−118.
(18) Rajeswari, S.; Prasanthi, T.; Sudha, N.; Swain, R. P.; Panda, S.; Goka, V. Natural polymers: A recent review. *World J. Pharm. Pharm. Sci.* **2017**, *6*, 472−494.
(19) Kulkarni Vishakha, S.; Butte Kishor, D.; Rathod Sudha, S. Natural polymers—A Comprehensive review. *Int. J. Res. Pharm. Biomed. Sci.* **2012**, *3*, 1597−1613.
(20) Mahanta, R. Sustainable Polymers and Applications. In *Sustainable Polymers*; Pan Stanford Publishing: Danvers, USA, 2016; pp 1−57.
(21) Mertl-Millhollen, A. S.; Rambeloarivony, H.; Miles, W.; Kaiser, V. A.; Gray, L.; Dorn, L. T.; Williams, G.; Rasamimanana, H. The Influence of Tamarind Tree Quality and Quantity on *Lemur catta* Behavior. In *Ringtailed Lemur Biology: Lemur Catta in Madagascar*; Springer, 2006; pp 102−118.
(22) Joseph, J.; Kanchalochana, S. N.; Rajalakshmi, G.; Hari, V.; Durai, R. D. Tamarind seed polysaccharide: a promising natural excipient for pharmaceuticals. *Int. J. Green Pharm.* **2012**, *6* (4), 270−278.
(23) Castro, M. A. d.; Prata, W. M.; Cunha, A. S. Tamarind seed polysaccharide (TSP) uses in ophthalmic drug delivery. *Rev Ciênc Farm Básica Apl* **2022**, *43*, 1−10.
(24) Ghosh, S. K.; Pal, T. Interparticle coupling effect on the surface plasmon resonance of gold nanoparticles: from theory to applications. *Chem. Rev.* **2007**, *107*, 4797−4862.
(25) Mehata, M. S. Green route synthesis of silver nanoparticles using plants/ginger extracts with enhanced surface plasmon resonance and degradation of textile dye. *Mater. Sci. Eng.* **2021**, *273*, No. 115418.
(26) Kesharwani, P.; Jain, K.; Jain, N. K. Dendrimer as nanocarrier for drug delivery. *Prog. Polym. Sci.* **2014**, *39*, 268−307.
(27) Thakuria, A.; Kataria, B.; Gupta, D. Nanoparticle-based methodologies for targeted drug delivery-an insight. *J. Nanopart. Res.* **2021**, *23*, 1−30.
(28) Hammami, I.; Alabdallah, N. M. Gold nanoparticles:Synthesis properties and applications. *J. King Saud Univ., Sci.* **2021**, *7*, No. 101560.
(29) Kang, H.; Buchman, J. T.; Rodriguez, R. S.; Ring, H. L.; He, J.; Bantz, K. C.; Haynes, C. Stabilization of silver and gold nanoparticles: preservation and improvement of plasmonic functionalities. *Chem. Rev.* **2018**, *1*, 664−699.
(30) Ebara, M.; Uto, K. Gold Nanomaterials for Gene Therapy. In *Polymers and Nanomaterials for Gene Therapy*; Elsevier, 2016; pp 189−214.
(31) Akilandaeaswari, B.; Muthu, K. Green method for synthesis and characterization of gold nanoparticles using *Lawsonia interimis* seed extract and their photocatalytic activity. *Mater. Lett.* **2020**, *277*, No. 128344.
(32) Yadi, M.; Mostafavi, E.; Saleh, B.; Davaran, S.; Aliyeva, I.; Khalilov, R.; Nikzamir, M.; Nikzamir, N.; Akbarzadeh, A.; Panahi, Y.; Milani, M. Current developments in green synthesis of metallic nanoparticles using plant extracts: a review. *Artif. Cells, Nanomed., Biotechnol.* **2018**, *46*, S336−S343.
(33) Yulizar, Y.; Utari, T.; Ariyanta, H. A.; Maulina, D. Green method for synthesis of gold nanoparticles using *Polyscias scutellaria* leaf extract under UV light and their catalytic activity to reduce methylene blue. *J. Nanomater.* **2017**, *2017*, 1−6.
(34) Biswal, S. K.; Parida, U. K.; Bindhani, B. K. Gold nanoparticles capped with tamarind seed polysaccharide blended with chitosan composite for the growth of phosphate mineral. *Int. J. Cur. Eng. Technol.* **2013**, *3*, 104−1108.
(35) Joint, F. A. O. World Health Organization, and WHO Expert Committee on Food Additives. In *Evaluation of Certain Food Additives: Eighty-Fourth Report of the Joint FAO*; World Health Organization, 2017; p 78. ISBN 978-92-5-130021-3.
(36) Subramanian, E.; Santhanamari, P.; Murugan, C. Sensor functionality of conducting polyaniline-metal oxide (TiO_2/SnO_2) hybrid materials films toward benzene and toluene vapors at room temperature. *J. Electron. Mater.* **2018**, *47*, 4764−4771.
(37) Rashmi, M.; Arora, S. C.; Rajesh, M. Tamarind seed polysaccharide and its modifications—versatile pharmaceutical excipients—a review. *Int. J. Pharm. Technol. Res.* **2014**, *6*, 412−420.
(38) Feng, X.; Yang, G.; Xu, Q.; Hou, W.; Zhu, J. J. Self-assembly of polyaniline/Au composites: from nanotubes to nanofibers. *Macromol. Rapid Commun.* **2006**, *27*, 31−36.
(39) Sumathi, S.; Ray, A. R. Release behaviour of drugs from tamarind seed polysaccharide tablets. *J. Pharm. Pharm. Sci.* **2002**, *5*, 12−18.
(40) Bahram, M.; Mohammadzadeh, E. Green synthesis of gold nanoparticles with willow tree bark extract: a sensitive colorimetric sensor for cysteine detection. *Anal. Methods* **2014**, *17*, 6916−6924.
(41) Korotcenkov, G.; Cho, B. K. Thin film SnO_2-based gas sensors: film thickness influence. *Sens. Actuators, B* **2009**, *142*, 321−330.
(42) Tagad, C. K.; Rajdeo, K. S.; Kulkarni, A.; More, P.; Aiyer, R. C.; Sabharwal, S. Green synthesis of polysaccharide stabilized gold

https://doi.org/10.1021/acsomega.3c09137
ACS Omega 2024, 9, 10640−10649

nanoparticles: chemo catalytic and room temperature operable vapor sensing application. *RSC Adv.* **2014**, *4*, 24014.
(43) Basiri, S.; Mehdinia, A.; Jabbari, A. A sensitive triple colorimetric sensor based on plasmonic response quenching of green synthesized silver nanoparticles for determination of Fe^{2+}, hydrogen peroxide, and glucose. *Colloids Surf., A* **2018**, *545*, 138−146.
(44) Cai, Z.; Goo, E.; Park, S. Synthesis of tin dioxide (SnO2) hollow nanospheres and its ethanol-sensing performance augmented by gold nanoparticle decoration. *J. Alloys Compd.* **2021**, *883*, No. 160868.
(45) Çapan, R.; Goktas, H.; Ozbek, Z.; Sen, S.; Ozel, M. E.; Davis, F. Langmuir−Blodgett thin film for chloroform detection. *Appl. Surf. Sci.* **2015**, *350*, 129−134.

https://doi.org/10.1021/acsomega.3c09137
ACS Omega 2024, 9, 10640−10649